



ELSEVIER

Available online at www.sciencedirect.com

SCIENCE @ DIRECT®

Physics Letters A 314 (2003) 409–427

PHYSICS LETTERS A

www.elsevier.com/locate/pla

Global modeling of the Rössler system from the z -variable

Claudia Lainscsek^{a,*}, Christophe Letellier^b, Irina Gorodnitsky^a

^a *Cognitive Science Department, University of California at San Diego, 9500 Gilman Drive, La Jolla, CA 92093-0515, USA*

^b *CORIA UMR 6614, Université de Rouen Site Universitaire du Madrillet, Avenue de l'Université, BP 12 F-76801 Saint-Etienne du Rouvray cedex, France*

Received 29 October 2002; received in revised form 21 May 2003; accepted 27 May 2003

Communicated by C.R. Doering

Abstract

Obtaining a global model from the z -variable of the Rössler system is considered to be difficult because of its spiky structure. In this Letter, a 3D global model from the z -variable is derived in a space spanned by the state variable of the time-series itself and generic functions of the other two state variables. We term this space the Ansatz Space. The procedure consists of two steps. First, models built in the derivative coordinates are obtained. Second, we use the analytical form of the map φ between systems in the original state space and in the differential space to find a class of models in the Ansatz Space. We find eight models in this class which we show to be dynamically equivalent to the original Rössler system. The important attribute of this approach is that we do not need to use any prior knowledge of the dynamical system other than the measured time series data in order to obtain global models from a single time series.

© 2003 Elsevier B.V. All rights reserved.

1. Introduction

The topic of this Letter is how to obtain a set of differential equations for the phase portrait reconstructed from a single time series. In particular, we are interested in obtaining a set of differential equations containing the minimal number of terms necessary to describe the underlying dynamics. The pioneering works by Takens [1], Packard et al. [2], and Sauer et al. [3] provide the theoretical background for reconstructing the phase portrait from recorded scalar time series. Crutchfield and McNamara [4] used such reconstructed phase space to find global models built on

delay or derivative coordinates. Principal components can also be used for reconstruction as introduced by Broomhead and King [5]. Gibson et al. [6] showed that the relationships between delays, derivatives and principal components consist of rotations and rescalings under certain conditions. These coordinate sets are therefore equivalent although a set may sometimes be superior to another for numerical reasons. Here we use embeddings as a tool to derive a model in a space spanned by the state variable of the time-series itself and generic functions of the other two state variables rather than in the embedding space. This is done using the so-called Ansatz Library [7]. We call the reconstructed space Ansatz Space.

In theory, any time series generated by a dynamical system could be used for modeling. In practice, it has been observed that even noise-free, infinite time

* Corresponding author.

E-mail address: clainscsek@ucsd.edu (C. Lainscsek).

series may not contain enough information to obtain all the dynamical properties from a scalar time series [8–10]. More recently, an observability index has been introduced to quantify the “observability” of the dynamics from a scalar time series [11]. A small index indicates small information content and a great difficulty in obtaining a global model. Under this index, the observability of the Rössler system from its three variables is ordered as $y \triangleright x \triangleright z$, where \triangleright means “provides a better observability of the underlying dynamics than”. According to this index, the y -variable is the easiest one from which one can obtain a model while the z -variable is the most difficult. There exist only a few published attempts to obtain a model from the z -variable of the Rössler system. Such a non-equivalence between the dynamical variables is valid for any modeling technique which can be divided in two main classes. In the first class the dimension of the phase space is fixed [12,13]. In this case, the number of terms, the number of monomials in a polynomial expansion, is varied. Usually, increasing the number of terms decreases the quality of the model and structure selection techniques must be used. The second class uses discrete-time models with cylindrical basis functions [14] which are less sensitive to an increase of number of terms. These “strong approximation” techniques have advantages and disadvantages for particular data sets. Using a global modeling technique of the first type, a 4D model with a quite large number of coefficients [11] was obtained. The single 3D model was found in [15], where the authors had to use an ad hoc structure selection by identifying the fixed point coordinates. This approach is not general and must be tailored to the time series at hand. The resulting model [15] contains a large number of spurious terms which, besides making the model unnecessarily complex, induces numerical instabilities when integrated.

This Letter presents a different approach to structure selection. We describe a step-by-step process for obtaining 3D global models in the Ansatz Space rather than in the embedding space from time series of the z -variable of the Rössler system using an Ansatz Library based structure selection procedure [7]. The Ansatz Library, first introduced in [7], consists of the set of all analytically derivable maps between sets of ordinary differential equations of polynomial form and differential models expressed in terms of Lie derivatives, for

which we fix the number of state variables and the order of nonlinearity of polynomials. We show how this Ansatz Library can be used to preselect candidate differential models estimated from time series. The Letter details the computational strategy used to select plausible differential models. To circumvent estimation problems due to the spiky nature of the z -variable of the Rössler system, we propose an approach where we use the stability of the estimated model coefficients over a range of windows as the criteria to select candidate models. Since the Ansatz Library lists all possible maps between the polynomial dynamical models and the corresponding differential models, an inversion of these maps yields a set of equivalent but algebraically simpler models. Another novel computational method employed in this Letter is an iterative genetic algorithm combined with Newton’s method which is used to invert the maps between the differential models and the corresponding ansatz models. Using such a procedure, we identify eight dynamically equivalent 3D global models that capture the dynamics of the Rössler system observed from the z -variable. Of those eight, three models are minimum term models containing only seven terms and the other five contain eight or nine terms each. We show that these models are equivalent under a coordinate transformation which is identified.

The Letter is organized as follows. In Section 2 we describe how models in the differential space spanned by the derivative coordinates using an Ansatz Library are obtained. In Section 3, we describe how the best differential models are transformed into the space spanned by the z -variable with which we and linear functions of the other two state variables, using an iterative genetic algorithm. Section 4 presents the conclusion. For the remainder of the Letter, we will designate the variables of the Rössler system as (u_1, u_2, u_3) rather than (x, y, z) . The Letter focuses on the theoretical aspects of model reconstruction when the time series is free of noise contamination. Extensions of this method to noisy data are necessary for dealing with real world problems and will be published separately.

2. Modeling in the differential space

In this section we provide background to explain how we use an Ansatz Library to obtain models in

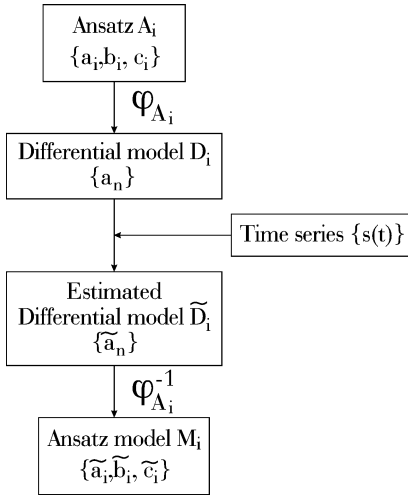


Fig. 1. Relationship between the ansatz A_i , the differential model D_i , the estimated differential model \tilde{D}_i and the ansatz model \mathcal{M}_i .

the differential space spanned by the derivative coordinates. Fig. 1 illustrates the relationship between the ansatz A_i , the differential models D_i , and the ansatz models \mathcal{M}_i that we use in our model identification procedure.

The Ansatz Space is related to the original state space through generic transformations of the unobserved state variables. The observed state variable is preserved [16].

2.1. Differential model

A general form of the differential model in terms of monomials is described here. For the sake of clarity, we limit the presentation to the case of 3D systems but the technique can be similarly extended to higher-dimensional systems. Let us consider a time-continuous dynamical system in $\mathbb{R}^3(u_1, u_2, u_3)$:

$$\begin{aligned} \dot{u}_1 &= f_1(\mathbf{u}), \\ \dot{u}_2 &= f_2(\mathbf{u}), \\ \dot{u}_3 &= f_3(\mathbf{u}), \end{aligned} \tag{1}$$

and let $s = h(\mathbf{u})$ be an observed scalar signal, where $h : \mathbb{R}^3 \rightarrow \mathbb{R}$ is a smooth function. The Lie derivative $L_f h(\mathbf{u})$ of the function $h(\mathbf{u})$ with respect to $f(\mathbf{u})$ is defined as

$$L_f h(\mathbf{u}) = \sum_{k=1}^3 f_k(\mathbf{u}) \frac{\partial h(\mathbf{u})}{\partial u_k}, \tag{2}$$

and recursively for the higher-order derivatives $L_f^j h(\mathbf{u}) = L_f(L_f^{j-1} h(\mathbf{u}))$. Using successive Lie derivatives we can build a model from the scalar signal s as follows:

$$\begin{aligned} X &= s = h(\mathbf{u}), \\ Y &= L_f h(\mathbf{u}), \\ Z &= L_f^2 h(\mathbf{u}). \end{aligned} \tag{3}$$

The phase portrait can thus be reconstructed in the differential space $\mathbb{R}^3(X, Y, Z)$. With these coordinates, a model from the recorded scalar signal can be obtained via a global modeling procedure. A general form for the model is given by

$$\begin{aligned} \dot{X} &= Y, \\ \dot{Y} &= Z, \\ \dot{Z} &= F(X, Y, Z, \alpha_n) = \sum_{n=1}^{N_\alpha} \alpha_n P_n, \end{aligned} \tag{4}$$

where α_n are the coefficients of the model function F to be estimated and P_n are the monomials $X^i Y^j Z^k$ [12]. The indices (i, j, k) for monomials may also be negative yielding a model with rational monomials. System (4) is called the *differential model*, and its parameters can be obtained by solving an overdetermined system of N equations with N_α unknown coefficients α_n ($N \gg N_\alpha$) using a least-square type method. N is the number of points retained for coefficient estimation, as discussed later.

2.2. Ansatz Library

The standard approach to choose the set of monomials P_n in (4) is to truncate a Taylor expansion at a given order. Such approach frequently introduces spurious terms in the models which decreases their quality. To circumvent this problem, various structure selections techniques have been proposed. As shown in [13], such structure selection algorithms can be useful in reducing the complexity of the model and in increasing its quality. Error Reduction Ratio (ERR) is an example of a structure selection method which has been implemented in [17] but the drawback of the technique is that it must use a global model as a starting point. Consequently, if it is not possible to obtain

a global model with a dynamics quite close to the investigated dynamics, this structure selection technique cannot be applied.

The structure selection strategy presented here is different from earlier structure selection attempts. Rather than to modify or build the structure of an obtained model, we apply a structure selection to identify the relevant coefficients among all the terms in the differential models D_i belonging to the Ansatz Library made of all putative models for a given order of nonlinearity and a given dimension. This is done using the stability of the coefficients over windows. Then, the coefficients are estimated from a given time series.

The first library made of six ansatz A_l ($l = 1, 2, 3, 18, 19, 21$) for defining the structure of 3D differential models was built in Ref. [7]. An extended Ansatz Library of systems of ODEs in a three-dimensional phase space was built in [18] for the case when the right-hand sides can be written as polynomials containing up to second order nonlinearities. We briefly detail how this library was built.

A 3D system of ODEs with the right-hand sides containing polynomials with up to second-order nonlinearities can be written in a general form as

$$\begin{aligned}\dot{x} &= a_0 + a_1x + a_2y + a_3z \\ &\quad + a_4x^2 + a_5xy + a_6xz \\ &\quad + a_7y^2 + a_8yz + a_9z^2, \\ \dot{y} &= b_0 + b_1x + b_2y + b_3z \\ &\quad + b_4x^2 + b_5xy + b_6xz \\ &\quad + b_7y^2 + b_8yz + b_9z^2, \\ \dot{z} &= c_0 + c_1x + c_2y + c_3z \\ &\quad + c_4x^2 + c_5xy + c_6xz \\ &\quad + c_7y^2 + c_8yz + c_9z^2.\end{aligned}\quad (5)$$

To derive the Ansatz Libraries in [18] we restrict the terms of the differential model to the set of all monomials of the form $X^i Y^j Z^k$, where i, j and k are integers, positive or negative. Since the order of the differential equations is interchangeable. We fix the x -variable as the observable in all cases, i.e., $s = x$, to obtain a set of non-redundant libraries. We then find which model structures would allow us to invert the maps φ_l to express the coefficients $\{\alpha_{n,l}\}$ of the differential models D_l (l is the index

of the l th differential model of the library) in terms of the coefficients $\{a_i, b_j, c_k\}$ from Eq. (5). Through this process we find which coefficients (a_i, b_j, c_k) in Eq. (5) must be zero for the individual differential model structures. In the end we obtain a set of ODEs containing a limited number of terms for which the coefficients $\{a_j, b_k, c_l\}$ are nonzero. Note, that we do not use data to build the library.

The library for the case of second order nonlinearities consists of 26 such model structures listed in Table 1. In Table 2, the monomials involved in the differential models D_l corresponding to the 26 ansatz A_l reported in Table 1 are listed. Note, that the equations in this library are also referred to as jerky dynamics in the literature. Attempts to build a complete jerky dynamics library were presented in [19], but that library was able to capture only a part of our list.

The objective of our procedure is to select the best differential model D_l which captures accurately the dynamics under investigation. In order to do this, we start with the structure resulting from the concatenation of the 26 differential models $\{D_l\}_{l=1}^{26}$ which reads as follows:

$$\begin{aligned}\dot{X} &= Y, \\ \dot{Y} &= Z, \\ \dot{Z} &= \alpha_1 + \alpha_2 \frac{1}{X^4} + \alpha_3 \frac{1}{X^3} + \alpha_4 \frac{1}{X^2} \\ &\quad + \alpha_5 \frac{1}{X} + \alpha_6 X + \alpha_7 X^2 + \alpha_8 X^3 \\ &\quad + \alpha_9 X^4 + \alpha_{10} X^5 + \alpha_{11} X^6 \\ &\quad + \alpha_{12} X^7 + \alpha_{13} X^8 + \alpha_{14} \frac{1}{Y} + \alpha_{15} \frac{X}{Y} \\ &\quad + \alpha_{16} \frac{X^2}{Y} + \alpha_{17} \frac{X^3}{Y} + \alpha_{18} \frac{X^4}{Y} \\ &\quad + \alpha_{19} \frac{X^5}{Y} + \alpha_{20} \frac{X^6}{Y} + \alpha_{21} Y \\ &\quad + \alpha_{22} \frac{Y}{X^4} + \alpha_{23} \frac{Y}{X^3} + \alpha_{24} \frac{Y}{X^2} \\ &\quad + \alpha_{25} \frac{Y}{X} + \alpha_{26} XY + \alpha_{27} X^2 Y \\ &\quad + \alpha_{28} X^3 Y + \alpha_{29} X^4 Y + \alpha_{30} X^5 Y \\ &\quad + \alpha_{31} X^6 Y + \alpha_{32} Y^2 + \alpha_{33} \frac{Y^2}{X^4}\end{aligned}$$

Table 1

Ansatz Library for systems of ODEs with up to quadratic nonlinearities. Each line represents one general system of ODEs which can be represented as a differential model in the form of Eq. (4). An ‘x’ in the table indicates that the corresponding coefficient (a_i, b_j, c_k) from the general system Eq. (5) is present in the ansatz-model. The coefficients with blank entries are zero. Ansatz 1, 2, 3, 19, 20, and 21 were presented previously in [7]

Ansatz	a_0	a_1	a_2	a_3	a_4	a_5	a_6	a_7	a_8	a_9	b_0	b_1	b_2	b_3	b_4	b_5	b_6	b_7	b_8	b_9	c_0	c_1	c_2	c_3	c_4	c_5	c_6	c_7	c_8	c_9
A ₁	x	x	x		x						x	x	x		x	x	x	x			x	x	x	x	x	x	x	x	x	x
A ₂	x	x	x		x						x	x	x	x	x	x		x				x	x	x	x	x	x	x	x	x
A ₃			x								x	x	x		x	x		x	x			x	x	x	x	x	x	x	x	x
A ₄	x	x	x	x	x						x	x	x	x	x							x	x	x	x	x				
A ₅	x	x	x	x	x						x	x		x								x	x		x			x		
A ₆	x	x	x	x	x						x	x		x								x	x		x		x			
A ₇	x	x	x	x	x		x				x	x		x								x	x		x					
A ₈	x	x	x	x	x						x	x	x		x										x					
A ₉	x	x	x	x	x						x	x	x		x								x							
A ₁₀	x	x			x				x					x	x	x								x					x	
A ₁₁	x	x			x				x				x	x		x								x					x	
A ₁₂	x	x			x				x		x		x		x		x							x					x	
A ₁₃	x	x		x	x				x		x		x											x					x	
A ₁₄	x	x		x	x				x							x								x					x	
A ₁₅	x	x		x	x				x						x									x					x	
A ₁₆	x	x		x	x				x				x											x					x	
A ₁₇									x					x		x								x					x	
A ₁₈									x					x		x								x					x	
A ₁₉	x	x		x	x						x	x	x		x	x	x	x				x	x	x	x	x	x	x	x	x
A ₂₀	x	x		x	x						x	x	x	x	x	x						x	x	x	x	x	x	x	x	x
A ₂₁					x						x	x	x		x	x						x	x	x	x	x	x	x	x	x
A ₂₂	x	x		x	x	x					x	x		x									x	x		x			x	
A ₂₃	x	x		x	x	x					x	x		x									x	x		x	x			
A ₂₄	x	x		x	x	x					x	x		x									x	x		x	x			
A ₂₅	x	x		x	x	x					x	x		x									x	x	x		x			
A ₂₆	x	x		x	x	x	x				x	x		x									x	x		x				

$$\begin{aligned}
 & + \alpha_{34} \frac{Y^2}{X^3} + \alpha_{35} \frac{Y^2}{X^2} + \alpha_{36} \frac{Y^2}{X} & + \alpha_{63} \frac{X^3 Z}{Y} + \alpha_{64} YZ + \alpha_{65} \frac{YZ}{X^3} + \alpha_{66} \frac{YZ}{X^2} \\
 & + \alpha_{37} XY^2 + \alpha_{38} X^2 Y^2 + \alpha_{39} X^3 Y^2 & + \alpha_{67} \frac{YZ}{X} + \alpha_{68} XYZ + \alpha_{69} X^2 YZ + \alpha_{70} Y^2 Z \\
 & + \alpha_{40} X^4 Y^2 + \alpha_{41} Y^3 + \alpha_{42} \frac{Y^3}{X^4} & + \alpha_{71} \frac{Y^2 Z}{X^3} + \alpha_{72} \frac{Y^2 Z}{X^2} + \alpha_{73} \frac{Y^2 Z}{X} + \alpha_{74} Z^2 \\
 & + \alpha_{43} \frac{Y^3}{X^3} + \alpha_{44} \frac{Y^3}{X^2} + \alpha_{45} \frac{Y^3}{X} & + \alpha_{75} \frac{Z^2}{X^2} + \alpha_{76} \frac{Z^2}{X} + \alpha_{77} \frac{Z^2}{Y}. \tag{6}
 \end{aligned}$$

Because this differential model only contains terms leading to a 3D ansatz with up to quadratic nonlinearities, the presence of spurious terms in this model structure is already greatly reduced. Those remaining will be eliminated as discussed in the subsequent part of this Letter using the example of the Rössler system investigated from the u_3 variable. Further note that the Ansatz Library approach does not require the knowledge of the order of the nonlinearity in the system investigated. If the order is not known, one can use a li-

brary built with an order of nonlinearities higher than the one expected for the system, since our procedure can eliminate spurious model terms that we might obtain. A library for the case of polynomials containing up to third order nonlinearities was derived in [18], and libraries for 4th and higher order nonlinearities can be derived analogously. For the sake of simplicity in illustrating our method we use only the library obtained for the second order nonlinearities in the present work but the extension to libraries that capture higher order nonlinearities is straightforward.

Note that involving higher order of nonlinearities would increase the number of candidate terms when the concatenation of all possible models is used as detailed here. A more favorable approach may be to use candidate models D_l separately to reduce the number of involved terms as done in Ref. [7]. Nevertheless, note that since the terms used here are fractional, the number of situations which can be captured for a given order of nonlinearity is significantly increased compared to polynomial expansion as used in [12]. For higher dimensions the numerical estimation of the derivatives may also become problematic.

2.3. Selecting the best differential model

Starting from the scalar signal s , the coefficients $\{\tilde{\alpha}_n\}$ of the differential model (6) are estimated from segments of the recorded data by using a singular value decomposition [20]. The time series is split into N_w windows of N/N_w points each. The coefficients $\{\tilde{\alpha}_n\}$ are robust, i.e., remain more or less constant over different windows of the recorded time series, when they are relevant to capture the underlying dynamics. Thus we use the stability of $\tilde{\alpha}_n$'s over different windows to identify the appropriate structure for the differential model \tilde{D}_l which best matches the underlying dynamics.

To measure stability of coefficients we use the significance

$$S_n = \frac{|\mu(\tilde{\alpha}_n)|}{\sigma(\tilde{\alpha}_n)}, \quad (7)$$

where $\tilde{\alpha}_n$ designates the n th coefficient of the differential model (6) estimated over a window, $\sigma(\tilde{\alpha}_n)$ designates the standard deviation, and $\mu(\tilde{\alpha}_n)$ designates the mean value of the coefficients over the N_w windows. The n th coefficient is stable if α_n remains constant

over the N_w windows of the time series. A very similar procedure for removing spurious terms was also used by Bezruchko et al. [21]. Here, we use in addition a threshold s_t under which centers are retained for estimating the values of the selected coefficients. Such a new modeling parameter is very useful for spiky time series as it will be shown below. In fact, the threshold helps to improve the coefficient estimation (once they are selected) in retaining points not too far from the fixed point, that is for which the derivatives are well estimated. Moreover, since some monomials are rational with X or Y as denominator, data points for which $X = u_3$ and $Y = \dot{X}$ are too close to zero are not retained for estimating the model in order to avoid numerical errors. Thus, centers are retained over a domain of the phase space where the derivatives are quite well estimated: not too close to zero where they are very sensitive to numerical errors and not too far from the fixed points where the distances between two points is quite large and, consequently, where the derivatives are not sufficiently accurate. This is rather important for spiky time series which, by definition, present large amplitude oscillations during which the dynamics is significantly faster than in the neighborhood of the fixed point. This means that using points retained in a limited domain of the phase space is sufficient to capture the whole dynamics. In fact, using different data point windows without any threshold is sufficient for selecting the relevant coefficients but not for estimating them with accuracy. The use of this technique is illustrated in the next subsection in the case of the u_3 -variable of the Rössler system which is considered as a rather difficult test case in the literature.

2.4. Differential model from the u_3 variable of the Rössler system

Here we attempt to estimate a global model from the u_3 variable of the Rössler system [22] given by

$$\begin{aligned} \dot{u}_1 &= -u_2 - u_3, \\ \dot{u}_2 &= u_1 + au_2, \\ \dot{u}_3 &= b + Cu_3 + u_1u_3, \end{aligned} \quad (8)$$

using the structure selection technique we described. The time series u_3 is generated by integrating these equations with the control parameters $(a, b, C) = (0.398, 2.0, -4.0)$. The Rössler system thus generates

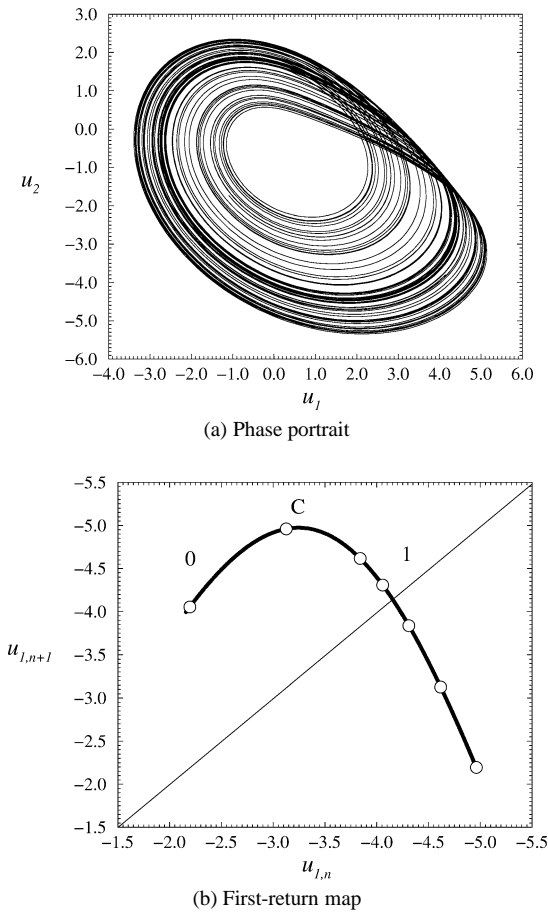


Fig. 2. Chaotic attractor generated by the Rössler system for $(a, b, C) = (0.398, 2.0, -4.0)$. The Poincaré section is computed using the half-plane $u_1 = -(C + \sqrt{C^2 + 4ab})/2$ with $\dot{u}_1 > 0$. A unimodal first-return map with a single critical point C characterizes its topology. The period-7 orbit which is the last created is also reported.

a chaotic attractor (Fig. 2(a)) which is characterized by a unimodal first-return map with a differentiable maximum (Fig. 2(b)). A refined characterization is given by the kneading sequence, i.e., the symbolic sequence of the last created periodic orbit, which is (1011110) for these control parameter values when the lowest period- p orbits ($p < 8$) are considered. It is a period-7 orbit which has 5 points in the decreasing branch of the first-return map and 2 in the increasing branch (Fig. 2(b)). The template of this Rössler attractor is a horseshoe template with a negative half-turn in the odd branch [23].

The spiky nature of the u_3 -variable presents a very challenging test case for a global modeling technique. Successful global models have been obtained for the cases when the recorded scalar signal is either $s = u_1$ or $s = u_2$, but not in the case when the recorded scalar signal corresponds to the u_3 -variable. In the latter case, no successful 3D model has been obtained without a strong structure selection that was specifically tailored to the time series [15] as we discussed above.

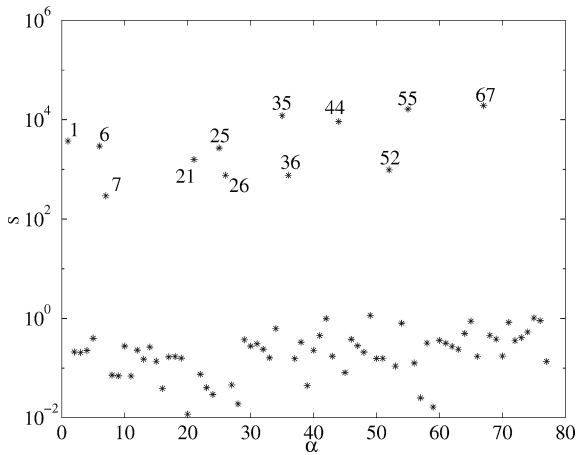
In order to obtain a differential model under the form (6), successive derivatives of the time series u_3 are required. A point of the time series, $s_i = u_3(i\delta t)$ where δt is the time step at which the time series is recorded is associated with its successive derivatives, thus $(X_i = u_3(i\delta t), Y_i = \dot{X}_i, Z_i = \ddot{X}_i, \dot{Z}_i = \dddot{X}_i)$ provides a so-called center. The first derivatives at the i th point of the time series are estimated according to

$$\dot{s}_i = \frac{M(M-1)}{2} \times \sum_{m=2}^M \sum_{n=1}^{m-1} \frac{m^3(s_{i+n} - s_{i-n}) - n^3(s_{i+m} - s_{i-m})}{2mn\delta t(m^2 - n^2)}, \tag{9}$$

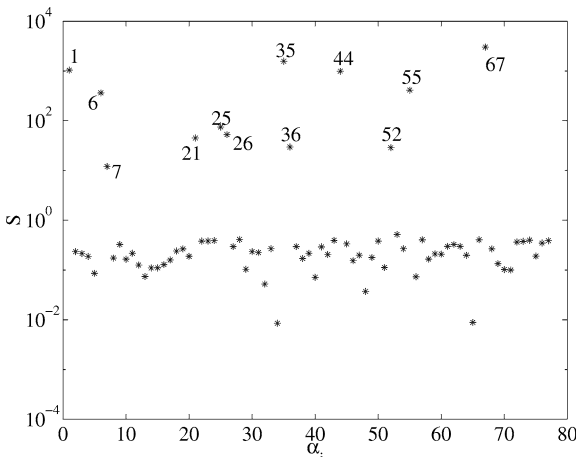
where $2M$ is the number of points to take into account. In this work, we use $M = 3$. The second and third derivatives are then computed from the first and second derivatives, respectively.

The stability of the estimated coefficient $\tilde{\alpha}_n$ is computed as previously defined. Note that the concatenation of the ansatz corresponding to quadratic nonlinearities and 3D systems is used here, which is the model structure (6). The significance is computed using 50 windows of 3000 data points each with a window shift of 750 points (Fig. 3(a)). Twelve coefficients are clearly more stable than the others. Note that our structure selection technique is sufficiently efficient to identify the relevant coefficients even from a very limited knowledge of the phase portrait. This is illustrated in the example where the Rössler system with $C = -5.9$ generates a period-1 limit cycle (Fig. 3(b)). The second step of the procedure may then be applied as described below and similar results are obtained. According to Table 2, indices of the stable coefficients are

{1, 6, 7, 21, 25, 26, 35, 36, 44, 52, 55, 67}.



(a) From a chaotic behavior $C = -4.0$



(b) From a limit cycle behavior $C = -5.9$

Fig. 3. Logarithm of the significance of the 77 coefficients $\tilde{\alpha}_n$ of the model (6) with indices as reported in Table 2. They are computed from a chaotic regime (a) and a period-1 limit cycle (b). In both cases, the same twelve coefficients are easily identified.

They refer to the monomials

$$\left\{ 1, X, X^2, Y, \frac{Y}{X}, XY, \frac{Y^2}{X^2}, \frac{Y^2}{X}, \frac{Y^3}{X^2}, Z, \frac{Z}{X}, \frac{YZ}{X} \right\}, \tag{10}$$

respectively (Table 2). Only models D_{19} and D_{20} contain all these terms.

The estimated differential model from the u_3 -variable of the Rössler system has therefore the struc-

ture:

$$\begin{aligned} \dot{X} &= Y, \\ \dot{Y} &= Z, \\ \dot{Z} &= \alpha_1 + \alpha_6 X + \alpha_7 X^2 + \alpha_{21} Y \\ &\quad + \alpha_{25} \frac{Y}{X} + \alpha_{26} XY + \alpha_{35} \frac{Y^2}{X^2} \\ &\quad + \alpha_{36} \frac{Y^2}{X} + \alpha_{44} \frac{Y^3}{X^2} \\ &\quad + \alpha_{52} Z + \alpha_{55} \frac{Z}{X} + \alpha_{67} \frac{YZ}{X}. \end{aligned} \tag{11}$$

It may be easily confirmed that this structure has in fact the structure of the differential system analytically computed from the u_3 -variable. Rather than using differential model D_{19} or D_{20} for estimating the numerical values of coefficients α_n , we prefer to use the twelve terms form (11): such a small set of coefficients will be helpful to ensure a better accuracy on the estimated coefficients $\tilde{\alpha}_n$. In order to do so, 10000 centers from the time series are randomly chosen under a threshold s_t . By varying the threshold value s_t , a plateau on which all the coefficients are fairly constant have been identified, that is for $s_t \in [0.4; 1.0]$. The mean values of the coefficients are estimated over 13 data sets corresponding different threshold s_t obtained by increasing s_t over the plateau $[0.4; 1.0]$ using a step equal to 0.05. The values of the twelve coefficients are reported in Table 3 where the theoretical values α_n of coefficients are also listed for comparison. The estimated coefficients have values very close to the theoretical ones. Note that the plateau corresponds to the domain of the u_3 -time series where all the maxima are excluded as centers used for estimating the model. This is equivalent to exclude the center for which derivatives are close to zero and not accurately estimated since the dynamics is too fast with respect to the sampling time. More accurate derivatives would require a higher sampling rate but in that case, the derivatives at centers located at small values of u_3 would be damaged by oversampling.

To validate the twelve terms differential model (11), it is integrated. It thus generates a period-7 limit cycle shown in Fig. 4(a). This does not mean that our estimated model is incorrect because a periodic window can often occur close to a chaotic attractor when one control parameter is varied slightly. In our

Table 2

Monomials of the differential models corresponding to the 26 ansatz reported in Table 1. An ‘x’ indicates that the monomial is present in the differential model. The gray boxes in the first row indicate the monomials α_i that are selected by our structure selection technique applied to the time series of the $s = u_3$ component of the Rössler system. The gray boxes in the table highlight the two differential models D_{19} and D_{20} that contain all the relevant monomials

Monomial	Ansatz																									
	1	2	3	4	5	6	7	8	9	10	11	12	13	14	15	16	17	18	19	20	21	22	23	24	25	26
1	1	x	x	x	x					x	x	x	x	x	x	x			x	x						
2	$1/X^4$																		x	x						
3	$1/X^3$																		x	x						
4	$1/X^2$																		x	x						
5	$1/X$	x																	x	x						
6	X	x	x	x	x	x	x			x	x	x	x	x	x	x			x	x	x			x	x	
7	X^2	x	x	x	x	x	x		x	x	x	x	x	x	x	x			x	x	x	x	x	x	x	x
8	X^3	x	x	x		x	x			x	x	x	x	x	x	x			x	x	x	x	x	x	x	x
9	X^4	x	x					x		x	x	x	x	x	x	x			x	x	x	x	x			
10	X^5	x	x																	x						
11	X^6	x	x																							
12	X^7	x	x																							
13	X^8		x																							
14	$1/Y$			x																						
15	X/Y			x																						
16	X^2/Y			x																						
17	X^3/Y			x																						
18	X^4/Y			x																						
19	X^5/Y																									
20	X^6/Y																									
21	Y	x	x	x	x			x	x		x	x	x	x	x	x	x	x	x	x	x	x	x			x
22	Y/X^4																			x						
23	Y/X^3																			x	x					
24	Y/X^2																			x	x					
25	Y/X	x				x	x		x	x	x				x	x	x			x	x				x	
26	XY	x	x	x	x	x	x	x		x	x	x	x	x	x	x	x	x	x	x	x	x	x	x	x	x
27	X^2Y	x	x	x		x				x	x	x	x	x	x	x	x	x	x	x	x	x	x	x	x	x
28	X^3Y	x	x																		x					
29	X^4Y	x	x																							
30	X^5Y	x	x																							
31	X^6Y		x																							
32	Y^2	x	x	x	x			x	x			x	x			x		x	x	x	x	x	x			x
33	Y^2/X^4																			x						
34	Y^2/X^3																			x	x					
35	Y^2/X^2																			x	x		x	x	x	x
36	Y^2/X	x				x	x		x	x	x	x			x	x	x			x	x			x		
37	XY^2	x	x	x																	x					
38	X^2Y^2	x	x																							
39	X^3Y^2	x	x																							
40	X^4Y^2		x																							
41	Y^3	x	x	x																						
42	Y^3/X^4																				x					
43	Y^3/X^3																				x	x				
44	Y^3/X^2																				x	x		x	x	x
45	Y^3/X	x																								
46	XY^3	x	x																							

(continued on next page)

Table 2 (continued)

	Monomial	Ansatz																									
		1	2	3	4	5	6	7	8	9	10	11	12	13	14	15	16	17	18	19	20	21	22	23	24	25	26
47	X^2Y^3		x																								
48	Y^4		x																								
49	Y^4/X^4																			x							
50	Y^4/X^3																				x						
51	Y^4/X	x																									
52	Z	x	x	x	x	x	x		x	x	x	x	x	x	x	x	x	x	x	x	x	x			x		
53	Z/X^3																			x							
54	Z/X^2																			x	x						
55	Z/X	x																		x	x		x	x	x	x	
56	XZ	x	x	x	x	x	x		x	x	x	x	x	x	x	x	x	x	x	x	x	x	x	x	x	x	
57	X^2Z	x	x																		x						
58	X^3Z	x	x																		x						
59	X^4Z		x																								
60	Z/Y			x				x																			x
61	XZ/Y			x				x															x				x
62	X^2Z/Y			x				x															x				x
63	X^3Z/Y							x															x				x
64	YZ	x	x	x																							
65	YZ/X^3																				x						
66	YZ/X^2																				x	x					
67	YZ/X	x				x	x		x	x	x	x			x	x	x			x	x	x	x	x	x	x	
68	XYZ	x	x																								
69	X^2YZ		x																								
70	Y^2Z		x																								
71	Y^2Z/X^3																				x						
72	Y^2Z/X^2																					x					
73	Y^2Z/X	x																									
74	Z^2		x																								
75	Z^2/X^2																				x						
76	Z^2/X	x																				x					
77	Z^2/Y			x				x															x				x

Table 3

Estimated coefficients of the differential model (11) made of the twelve more stable coefficients. The coefficients are averaged over 13 data sets corresponding to different values of the threshold $s_t \in [0.4; 1.0]$ sampled at 0.05 increment. Theoretical values α_n are also reported for comparison

n	1	6	7	21	25	26	35	36	44	52	55	67
α_n	2.0	-4.0	0.398	-1.0	0.796	-1.0	4.0	-0.398	-2.0	0.398	-2.0	3.0
$\tilde{\alpha}_n$	1.9982	-3.9901	0.3906	-0.9986	0.7944	-1.0043	3.9957	-0.3900	-1.9958	0.3959	-1.9976	2.9965

case, a periodic cycle is due to slight departures between the estimated coefficients and the analytical ones (see Table 3). To investigate whether the limit cycle corresponds to a periodic window close to the original chaotic attractor, we slightly increase the first parameter $\tilde{\alpha}_1$ from 1.9982 to 1.999, which results in a chaotic attractor shown in Fig. 4(b). From its first-return map (Fig. 4(c)), the period-7 limit cycle is encoded by (1011110), which is the

same symbolic sequence than the kneading sequence previously identified on the original chaotic attractor (Fig. 2(b)). Moreover, it can be shown that the attractor in Fig. 4(b) is characterized by the same template as the original Rössler system. The obtained model is therefore very close to the original dynamics, but it is built in the phase space spanned by the Lie derivatives $\mathbb{R}^3(X, Y, Z)$ rather than in the original phase space $\mathbb{R}^3(u_3, u_1, u_2)$.

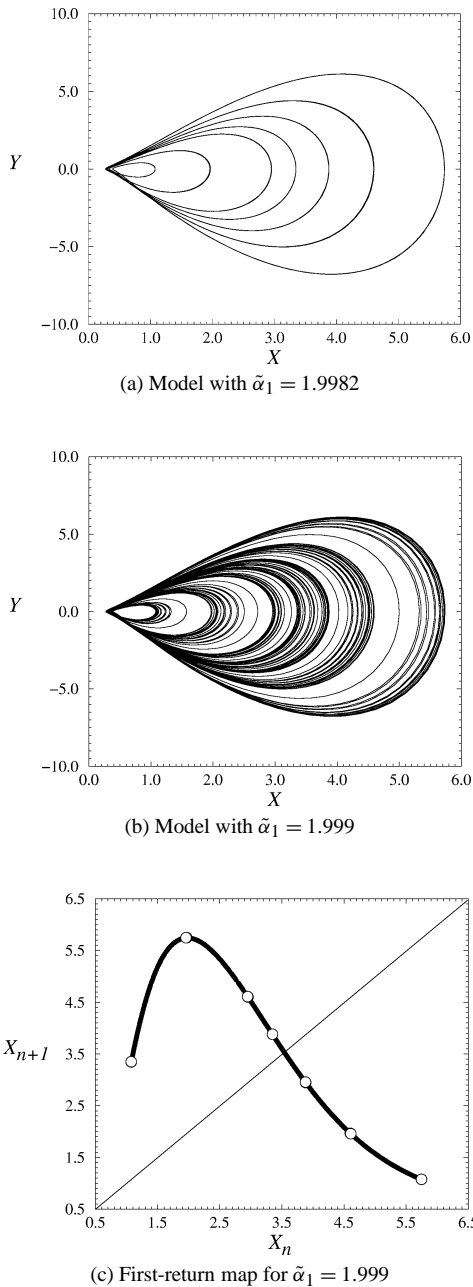


Fig. 4. Phase portraits of the differential model (11) and the differential model for which coefficient $\tilde{\alpha}_1$ is slightly modified. The first-return map of the latter is also shown. The period-7 limit cycle (symbols “o” in the first-return map represent the location of the seven periodic point of this orbit) is encoded by the same symbolic sequence than the kneading sequence of the Rössler attractor. The model dynamics is therefore very close to the dynamics of the original Rössler system.

The use of the Ansatz Library allows for significant improvement in the use of the coefficient stability for structure selection and for estimating their values. This improvement is obvious when the structure of the differential model to estimate corresponds to one in the library.

When this is not the case, some transformation on the time series may be applied to handle the situation. This is illustrated briefly in Appendix B for the u_1 -variable of the Rössler system. In this example, the transformation is a simple shift which renders this time series part of the Ansatz Library. However, when such a transformation cannot be found, standard modeling techniques remain applicable as in the case of y - and z -variable of the Lorenz system.

3. Estimating a model in the Ansatz Space

Our next objective is to obtain a model in the space $\mathbb{R}^3(x, y, z)$ associated with the selected differential model (11). At this stage the transformation φ_i between the selected differential model (11), that is part of the two general differential models D_{19} and D_{20} , and the ansatz A_i ($i = 19, 20$) is inverted. In order to do this, only the monomials corresponding to the twelve significant coefficients in the models \tilde{D}_i are taken into account. Using a genetic algorithm based search described in Appendix A, 14 sets of coefficients for ansatz A_{19} induce the twelve term structure of the differential model D_{19} . All 14 sets have between 7 and 10 coefficients (the others being equal to zero) and ansatz A_{19} with all possible coefficients that correspond to the differential model (11) is

$$\begin{aligned} \dot{x} &= a_0 + a_1x + a_5xy, \\ \dot{y} &= b_0 + b_1x + b_2y + b_6xz, \\ \dot{z} &= c_0 + c_2y + c_3z. \end{aligned} \tag{12}$$

Among the 14 sets, 3 have only 7 terms.

For ansatz A_{20} , 156 sets of coefficients inducing the twelve term structure of the differential model D_{20} are found. The 156 sets have between 7 and 12 terms. Among them, 14 sets have 7 terms. Ansatz A_{20} with all possible coefficients that correspond to the differential

model (11) is

$$\begin{aligned}\dot{x} &= a_0 + a_1x + a_5xy, \\ \dot{y} &= b_0 + b_1x + b_2y + b_3z, \\ \dot{z} &= c_0 + c_1x + c_2y + c_3z + c_5xy.\end{aligned}\quad (13)$$

At this stage, we try to select only the terms necessary to capture the underlying dynamics. A seven-term ansatz model which contains the minimum number of terms of all models summarized in Eq. (13) could be sufficient to capture the underlying dynamics represented by our data. We thus first consider only the sets of seven coefficients for the ansatz A_{19} and A_{20} . Obviously, if in the course of the analysis we find that seven terms are not sufficient to obtain a satisfactory ansatz model, sets with a greater number of terms will be considered.

The 3 seven-term models corresponding to A_{19} and the 14 seven-term models corresponding to A_{20} lead to 17 sets of nonlinear equations that must be inverted independently in order to obtain a model in the Ansatz Space $\mathbb{R}^3(x, y, z)$. Each of these sets of nonlinear equations expresses the relationship between the coefficients $\tilde{\alpha}_n$ of the differential model and the ansatz coefficients $\{\tilde{a}_i, \tilde{b}_j, \tilde{c}_k\}$. The class of transformations associated with the models described by the reduced-form (12) for ansatz A_{19} is given by

$$\varphi_{A_{19}} = \begin{cases} \alpha_1 = a_0b_2c_3, \\ \alpha_6 = -a_0b_6c_2 - a_5b_0c_3 + a_1b_2c_3, \\ \alpha_7 = a_5b_6c_0 - a_1b_6c_2 - a_5b_1c_3, \\ \alpha_{21} = -a_5b_0 + a_1b_2 - b_2c_3, \\ \alpha_{25} = 2a_0b_2 + a_0c_3, \\ \alpha_{26} = b_6c_2, \\ \alpha_{35} = 3a_0, \\ \alpha_{36} = -2b_2 - c_3, \\ \alpha_{44} = -3, \\ \alpha_{52} = b_2 + c_3, \\ \alpha_{55} = -a_0, \\ \alpha_{67} = 4. \end{cases}\quad (14)$$

Similarly, the class of transformations associated with the ansatz models described by the reduced-form (13) for ansatz A_{20} is given by

$$\varphi_{A_{20}} = \begin{cases} \alpha_1 = -a_0b_3c_2 + a_0b_2c_3, \\ \alpha_6 = a_5b_3c_0 - a_1b_3c_2 - a_5b_0c_3 \\ \quad + a_1b_2c_3 - a_0b_3c_5, \\ \alpha_7 = a_5b_3c_1 - a_5b_1c_3 - a_1b_3c_5, \\ \alpha_{21} = b_3c_2 - b_2c_3, \\ \alpha_{25} = a_0b_2 + a_0c_3, \\ \alpha_{26} = a_5b_1 + b_3c_5, \\ \alpha_{35} = 2a_0, \\ \alpha_{36} = -b_2 - c_3, \\ \alpha_{44} = -2, \\ \alpha_{52} = b_2 + c_3, \\ \alpha_{55} = -a_0, \\ \alpha_{67} = 3. \end{cases}\quad (15)$$

In Eqs. (14) and (15) the additional equations $0 = f_m(a_i, b_j, c_k)$ with $m = 1, 2, \dots, 77$ and $m \neq \{1, 6, 7, 21, 25, 26, 35, 36, 44, 52, 55, 67\}$ are not listed since the vanishing coefficients (a_i, b_j, c_k) make the functions $f_m(a_i, b_j, c_k)$ zero. These equations therefore do not provide any additional information and can be excluded.

The transformations (14) and (15) are inverted using a genetic algorithm described in Appendix A. Such an algorithm provides an efficient way to solve a numerically ill-conditioned problem. Depending on the number of terms involved in the models, the problems may be over-determined or under-determined for some $\{\tilde{a}_i, \tilde{b}_j, \tilde{c}_k\}$. Such optimization problems tend to have many local minima and only a global search procedure such as a genetic algorithm allows to find the global minimum. The algorithm here proposed may also be used for a larger set of equations. Among other optimization criteria, the genetic algorithm is set up to reject models which are numerically unstable during integration. This is done by integrating the candidate models from a set of 10 randomly chosen initial conditions over 5000 integration steps. The model is rejected when none of this 10 integration remains within the interval $[-10^4; 10^4]$.

The genetic algorithm is set to minimize the least square error ρ as defined in Eq. (A.1) in order to invert the transformations φ_{19} and φ_{20} for the different sets of α_i corresponding to different thresholds s_t . We use a two step procedure. The first run of the genetic algorithm is used to separate the potentially good models from those producing a large misfit error. In this run the population is set to a small size and

no absolute convergence to the global minimum in the solution space is sought.

In the case of the differential models \tilde{D}_{19} , the coefficients $\tilde{\alpha}_{44}$ and $\tilde{\alpha}_{67}$ are estimated by the algorithm to be equal to -1.9958 and 2.9965 , respectively. These values are significantly different from the values of -3 and 4 for these terms given in (14). Consequently, we can see that the misfit error will always remain large and therefore ansatz A_{19} is rejected from further consideration.

In the case of the differential models \tilde{D}_{20} , the least square errors distribution for the 14 seven-term sets of coefficients is shown in Fig. 5. Observe that out of the 14 sets, three produce significantly lower residuals. The significant gap in the residual values serves as a preselection criterion and we limit our investigation to these three possible reduced forms from ansatz A_{20} which are

$$\mathcal{M}_6: \begin{cases} \dot{x} = a_0 + a_5xy, \\ \dot{y} = b_1x + b_3z, \\ \dot{z} = c_0 + c_2y + c_3z, \end{cases} \quad (16)$$

$$\mathcal{M}_{10}: \begin{cases} \dot{x} = a_0 + a_1x + a_5xy, \\ \dot{y} = b_1x + b_3z, \\ \dot{z} = c_2y + c_3z, \end{cases} \quad (17)$$

$$\mathcal{M}_{11}: \begin{cases} \dot{x} = a_0 + a_5xy, \\ \dot{y} = b_0 + b_1x + b_3z, \\ \dot{z} = c_2y + c_3z. \end{cases} \quad (18)$$

The coefficients $\tilde{a}_i, \tilde{b}_j, \tilde{c}_k$ in these models are found by performing the second genetic algorithm run. The following implementation features are utilized in the second run. The algorithm is initialized using the half of the numerically obtained coefficients from the first step that corresponds to the smallest residuals. In the subsequent iteration the values for the a_i, b_j, c_k that

are near those values found in the previous iteration are designed to be preferred by the genetic algorithm. For example, if the different values for coefficient a_0 are between 1.23 and 2.58 after the first iteration, values within these limits will have a greater survival rate in the second iteration. The algorithm also incorporates the Newton method to speed up convergence as described in Appendix A. Using this implementation, we obtain the coefficients $\tilde{a}_j, \tilde{b}_k, \tilde{c}_l$ for the models shown in Table 4. These three models generate chaotic attractors (Fig. 6) which are equivalent as proved below.

Note that model \mathcal{M}_{10} has the exact same structure of the original Rössler system (Eq. (8)). We show next that all three seven term models are related through a transformation which leaves the dynamics unchanged. First, we observe that from φ_{20} one can determine

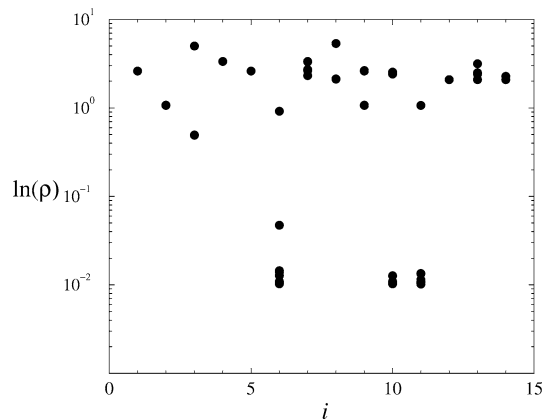


Fig. 5. Logarithm of the residuals (ρ) (see Eq. (A.1)) of the first run of the genetic algorithm for the 14 sets of coefficients for ansatz \tilde{A}_{20} . Each points correspond to the global error computed for a given value of the threshold s_t .

Table 4

Estimated coefficients for the 3 models obtained by inverting the transformation φ_{20} using the genetic algorithm. Model \mathcal{M}_{10} has the exact structure of the original Rössler system (Eq. (8)). Models \mathcal{M}_6 and \mathcal{M}_{11} are shown to be alternative representations of the Rössler system

Coefficient	Rössler system	Model \mathcal{M}_6	Model \mathcal{M}_{10}	Model \mathcal{M}_{11}
a_0	2.000	1.998	1.998	1.998
a_1	-4.000	.	-3.992	.
a_5	1.000	0.401	0.264	1.305
b_0	.	.	.	7.741
b_1	-1.000	-2.509	-3.808	-0.768
b_3	-1.000	2.271	0.337	-2.660
c_0	.	-4.381	.	.
c_2	1.000	-0.440	-2.966	0.376
c_3	0.398	0.395	0.395	0.395

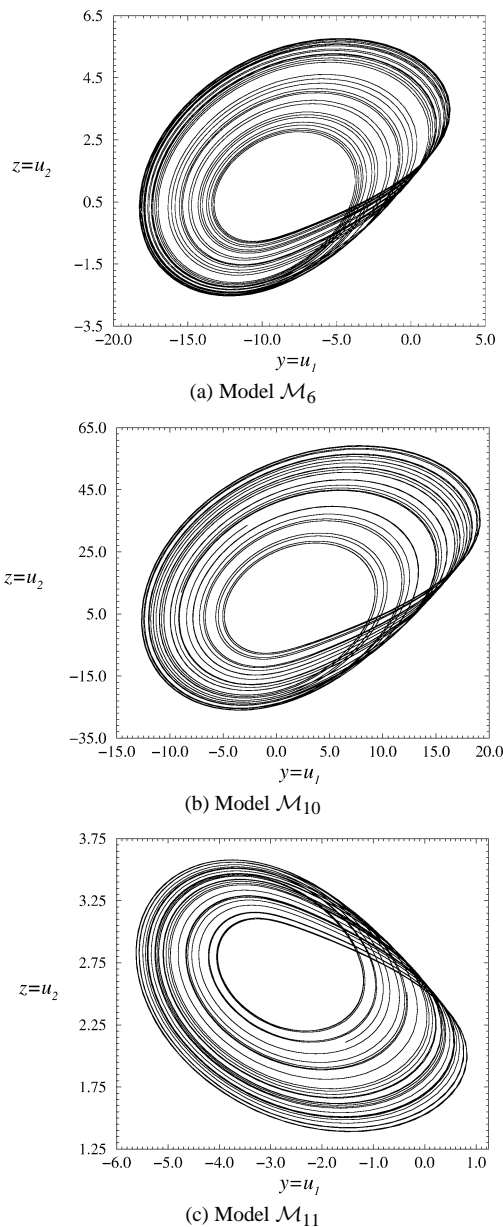


Fig. 6. Phase portraits associated with the three ansatz models. Plane projection in the yz -plane are shown.

only the products $b_3c_2 = -1$ and $a_5b_1 = -1$. In other words, one of these coefficients may be arbitrarily fixed until the second is chosen in order to satisfy a constant product. Such indetermination corresponds in fact to a rescaling of the y and z variables. When the coordinate transformation $(x, y, z) \mapsto (x, m\tilde{y} + n, j\tilde{z} + k)$ is applied to the original Rössler system

$((x, y, z) = (u_3, u_1, u_2)$ in Eq. (8))

$$\begin{aligned} \dot{x} &= b + Cx + xy, \\ \dot{y} &= -x - z, \\ \dot{y} &= y + az, \end{aligned} \tag{19}$$

it becomes

$$\begin{aligned} \dot{x} &= a_0 + (a_1 + na_5)x + ma_5x\tilde{y} \\ &= \tilde{a}_0 + \tilde{a}_1x + \tilde{a}_5x\tilde{y}, \\ \dot{\tilde{y}} &= \frac{kb_3}{m} + \frac{b_1}{m}x + \frac{jb_3}{m}\tilde{z} \\ &= \tilde{b}_0 + \tilde{b}_1x + \tilde{b}_3\tilde{z}, \\ \dot{\tilde{z}} &= \frac{nc_2 + kc_3}{j} + \frac{mc_2}{j}\tilde{y} + c_3\tilde{z} \\ &= \tilde{c}_0 + \tilde{c}_2\tilde{y} + \tilde{c}_3\tilde{z}. \end{aligned} \tag{20}$$

The parameters m and j in Eq. (20) are scaling parameters for the y and z coordinates. Depending on how the parameters n and k are chosen, different models with more than seven terms can also be obtained (see Table 5). The time evolution of these numerically integrated models is identical up to the scalings and displacements $y = m\tilde{y} + n$ and $z = j\tilde{z} + k$ when using the initial conditions $(x_0, \frac{y_0-n}{m}, \frac{z_0-k}{j})$. Thus, through this analytic transformation we identify five additional models besides the three models which we found computationally.

All eight models are dynamically equivalent to the original Rössler system and the five additional models containing either 8 or 9 terms could have been also obtained numerically by running the genetic algorithm on all 156 possible sets of coefficients for A_{20} . Note, that all 156 possible sets lead to the same differential model, but only the eight sets listed in Table 5 have the same values for the coefficients α_i which makes the identification of these alternative representations possible.

In fact, there exists an infinite number of models that produce the same time series. These models can be written as a generalization of Eq. (20),

$$\begin{aligned} \dot{x} &= \tilde{a}_0 + \tilde{a}_1x + \tilde{a}_5x\Phi_y, \\ \dot{\Phi}_y &= \tilde{b}_1x + \tilde{b}_3\Phi_z, \\ \dot{\Phi}_z &= \tilde{c}_2\Phi_y + \tilde{c}_3\Phi_z, \end{aligned} \tag{21}$$

where $\Phi_y = \Phi_y(y, z)$ and $\Phi_z = \Phi_z(y, z)$ are independent generic functions of the unobserved state variables. Therefore, reconstruction of dynamical systems

Table 5
 Ansatz models of Eq. (20) that are equivalent to the original Rössler system

	\mathcal{M}_6	\mathcal{M}_{10}	\mathcal{M}_{11}	8-term models			9-term models	
n	$-\frac{a_1}{a_5} = 4$	0	$-\frac{a_1}{a_5} = 4$	$-\frac{a_1}{a_5} = 4$	$\neq -\frac{a_1}{a_5}, \neq 0$	$\neq 0, \neq 4$	0	$\neq -\frac{a_1}{a_5}, \neq 0$
k	0	0	$-\frac{nc_2}{c_3}$	$\neq 0, \neq -\frac{nc_2}{c_3}$	0	$-\frac{nc_2}{c_3}$	$\neq 0, \neq -\frac{nc_2}{c_3}$	$\neq 0, \neq -\frac{nc_2}{c_3}$
a_0	2	2	2	2	2	2	2	2
$a_1 + na_5$		-4			$-4 + n$	$-4 + n$	-4	$-4 + n$
ma_5	m	m	m	m	m	m	m	m
$\frac{kb_3}{m}$			$\frac{4}{0.398m}$	$-\frac{k}{m}$		$\frac{n}{0.398m}$	$-\frac{k}{m}$	$-\frac{k}{m}$
$\frac{b_1}{m}$	$-\frac{1}{m}$	$-\frac{1}{m}$	$-\frac{1}{m}$	$-\frac{1}{m}$	$-\frac{1}{m}$	$-\frac{1}{m}$	$-\frac{1}{m}$	$-\frac{1}{m}$
$\frac{jb_3}{m}$	$\frac{j}{m}$	$\frac{j}{m}$	$\frac{j}{m}$	$\frac{j}{m}$	$\frac{j}{m}$	$\frac{j}{m}$	$\frac{j}{m}$	$\frac{j}{m}$
$\frac{nc_2+kc_3}{j}$	$\frac{4}{j}$			$\frac{4+0.398k}{j}$	$\frac{n}{j}$		$\frac{0.398k}{j}$	$\frac{n+0.398k}{j}$
$\frac{mc_2}{j}$	$\frac{m}{j}$	$\frac{m}{j}$	$\frac{m}{j}$	$\frac{m}{j}$	$\frac{m}{j}$	$\frac{m}{j}$	$\frac{m}{j}$	$\frac{m}{j}$
c_3	0.398	0.398	0.398	0.398	0.398	0.398	0.398	0.398

from a single time series is only possible in a space spanned by the time series itself and independent functions of the unobserved state variables. General results on such a class of models are postponed for future works.

4. Conclusion

Using a global modeling technique based on an Ansatz Library introduced in [7], a global model in the differential space and a model in the space associated with the chosen ansatz have been obtained from a scalar time series of the third coordinate of the Rössler system. The eight identified models are dynamically equivalent and three of the models are minimum term models containing seven terms only. These are the first models ever obtained for such a time series in 3D space without a prior knowledge on the structure of the model. Moreover, all spurious terms have been removed by a structure selection technique. Another important aspect of this technique is that a general class of model forms which capture the underlying dynamics can be identified.

Acknowledgements

C. Lainscsek and I. Gorodnitsky are supported by the NSF grant IIS-0082119. C. Lainscsek and

C. Letellier wish to thank the AMADEUS program and F. Schürer for encouraging this work.

Appendix A. Solving a system of nonlinear algebraic equations using a combined global and local search procedure

For finding the model in the Ansatz Space from a differential model, we need to solve a system of under- and simultaneously overdetermined nonlinear algebraic equations. This problem is solved by using combined global and local optimization procedures. The global search is performed with a Genetic Algorithm (GA) while the local search is realized by a Newton method as implemented in MATLAB.

A GA [24,25] is a global search algorithm that is based on natural genetics. A given problem is encoded as an array (population) of artificial strings (chromosomes). In the cases considered here where an optimization problem has to be solved, the guesses for possible solutions of a model are in the Ansatz Space. In our case, the chromosomes are strings of 1's and 0's. The GA manipulates this representation of the solution, but not the solution itself. A criterion for discriminating good from bad solutions according to the relative fitness of these solutions must be defined. This will be used to guide the evolution for future generations. The mean-square residual is here used as discrimination criterion.

After having encoded the problem in a chromosomal manner and having found a discrimination strategy for good solutions, an initial population of encoded solutions has to be created. This is accomplished by using a generator of random numbers without any prior knowledge of possibly good solutions. The initial population is in fact a set of random guesses for the optimal solution.

The evolution of this initial population towards later generations is obtained by applying genetic operators in an iterative process. The most common genetic operators are (1) selection, (2) recombination, (3) mutation, (4) elitism, and (5) junk [24,25]. Selection allocates greater survival for better individuals. Better solutions are preferred to worse ones. Additional new, possibly better individuals not present in the original population may be created via recombination and mutation. Recombination combines parental traits (bits) in a novel manner to form a better offspring. Mutation on the other hand modifies a single individual. It is a random walk in the neighborhood of a particular solution. Elitism guarantees that good solutions survive. By introducing junk, randomly generated individuals, into the new generation new blood is also introduced. Such a process helps to find the global minimum.

A sketch of our method can be found in Fig. 7. The color and shape notation is as follows. Round boxes correspond to genetic operators. Light boxes represent operations in the encoded binary space while dark boxes are connected to operations in the decimal parameter space. The one black box represents the local search part. The levels in the flow-chart indicated in Fig. 7 by circled boxes are described below.

1. An initial generation of $P_s = 600$ individuals, which are possible candidates for a solution of our problem, is generated using a random number generator. For the rest of the loop it is set to $P_s = 100$. The population size P_s is a critical parameter for running a GA. If it is chosen too small, no convergence in a reasonable time can be expected. If it is too big, the computations will slow down and each loop will take too long. To take this into account, the population size in our genetic algorithm will be dynamic. If big changes can be yielded from generation to generation, the number can be smaller than when the solution is trapped in a possible local minimum.

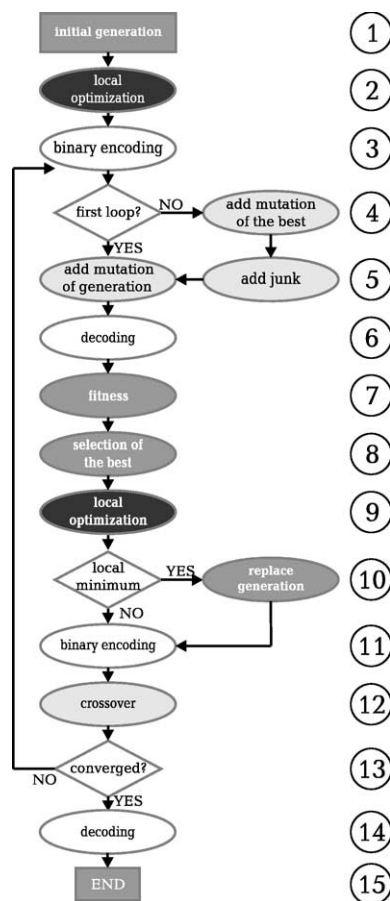


Fig. 7. Flow chart for solving a system of nonlinear algebraic equations using a GA (global search) combined with a Newton method (local optimization).

We also use another trick to keep the population size small. We let the GA run for each set of differential model coefficients α_n 's. Due to the range of the threshold s_t over which a plateau is observed, 13 different sets of coefficients are identified. Each of these GAs yield another solution, since the coefficients were computed from different parts of the set of data points. From these solutions we select the models with a significantly lower error and use them to determine coefficient range on which a second run of the GA will be performed. That means that the GA uses, for instance, values between 1.6 and 2.5 for coefficients a_0 during the second run. It turns out that some coefficients converge immediately to very small

fluctuations around the actual value, while others do not. This is an effect of the ill-defined problem to be solved.

2. After generating $P_s = 600$ individuals, a local Newton method is applied on 20 randomly chosen individuals. This number is a trade-off between efficiency and computation time, since running it on all of them would require too much time. This yields an initial population, which is a grid of local minima and completely random choices of our solution.
3. The individuals have to be encoded in a binary manner. Since a set of real numbers is to be encoded into a sequence of binary strings, an upper and a lower limit for possible numbers in our search space have to be chosen as well as the desired accuracy for these numbers. In our case, we use as the upper limit $L_u = 50$ and as the lower limit $L_l = -50$ and an accuracy of $A = 10^{-3}$. The encoding is continuous. This means that all possible

$$B = \text{Ceil} \left(\log_2 \left(\frac{L_u - L_l}{A} + 1 \right) + 3 \right)$$

bits for one real number are used for encoding. In other words, two binary strings can represent the same real number. Such a procedure does not effect the search, since the number of bits will be large. The added factors 1 and 3 are used to even out numerical uncertainties and to reduce the ambiguity of the continuous encoding.

Each individual consists of 12 real numbers corresponding to our 12 unknowns. Each of these real numbers are encoded in the previously described manner, which yields 12 strings of B 0's and 1's. They are then connected to one line of our population matrix. The P_s such lines form a $12 \cdot B \times P_s$ matrix, which corresponds to one population.

4. Starting from the second iteration mutated individuals of the winner of the former generation are added. This is done in two steps. In the first, one number is left constant and all others are mutated. In the second step only one number is mutated and all others are left constant. Mutations are done with a certain mutation probability. To avoid too low or to high mutation probabilities, it is randomly changed between 0.2 and 0.9 in each generation. Small mutation probabilities af-

fect small changes, while big mutations can yield big changes of the individuals.

5. To add new blood to each generation, randomly generated individuals, the so-called junks, are added to each generation.
6. The whole generation is mutated with a small mutation probability and added to the existing population.
7. In order to do the evaluation of our population in the next step, we have to decode the binary string matrix back to the space of real numbers.
8. The fitness f is the mean least square error

$$\rho = \sqrt{\sum_{i=1}^{i=12} (\tilde{\alpha}_i - \alpha_i)^2}, \tag{A.1}$$

where $\tilde{\alpha}_i$ are the estimated coefficients of the differential model while α_i are the coefficients obtained from the solution of equation (14) or (15) by the GA. Better individuals have a bigger chance to have more offspring while bad individuals die. To make a selection, better individuals get a higher selection number S_i ,

$$S_i = 100 \left(\frac{100 - (f_i - \min(f))}{f_{\max} - f_{\min}} \right)^3 \tag{A.2}$$

according to their fitness. Each individual is thus

$$C_i = \frac{P_s S_i}{\sum_{j=1}^{P_s} S_j}$$

times copied into the population ready for crossover.

9. The best individual could be a solution in the neighborhood of the global optimal solution. The GA would probably need a few generations to converge. To speed up this convergence, a Newton algorithm is applied to the winner of the former generation.
10. After watching runs of the GA for a couple of times a typical convergence time of about 5 iterations is used, if the population did not get trapped in a local minimum. The escape from such a local minimum can take a long time. To solve this convergence problem after 25 iterations, which corresponds to five times the typical convergence time, a completely new generation in the manner of levels 1 and 2 is

generated. The former unsuccessful generation is stored, but not used for 5 iterations. After that the new and the old generations are merged and used for further computations.

11. The population is again binary encoded.
12. Parts of the strings are exchanged between pairs of individuals to create new offspring. Better individuals will have more children.
13. Has the error changes for the last 10 generations?
14. To get the solution, the winner of the generation has to be decoded.
15. Stop the computations.

Appendix B. Modeling from the x -variable of the Rössler system

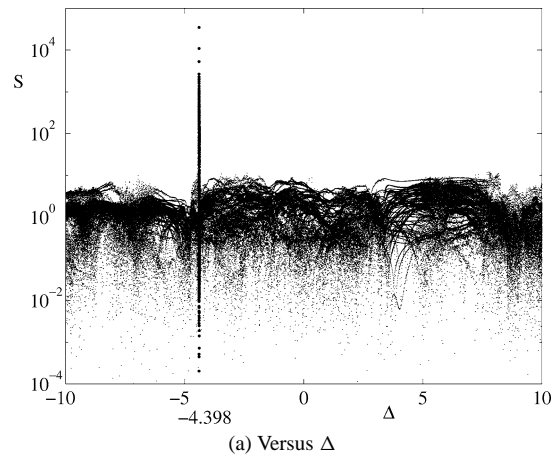
This appendix illustrates how the Ansatz Library can be used when the differential model is induced by a variable that has no corresponding ansatz in the library.

When the Rössler system is investigated from the u_1 -variable, there is no counterpart in our library. In such a case, our approach could remain unsuccessful since no coefficients are stable (case where $\Delta = 0$ in Fig. 8(a)). Nevertheless, we can apply a shift by $-\mathcal{C} + a$ to the u_1 -time series since it can be shown that an appropriate shift modifies the structure of the differential system induced by the u_1 -variable in such a way that it then belongs to the library. It is reasonable to assume that when the structure selection does not provide any obvious result, one can try simple transformations of the time series as e.g. applying a shift such as $s = u_1 + \Delta$. This was done for $\Delta \in [-10; 10]$ (Fig. 8(a)). A very clear singularity occurs for $\Delta = -4.398$ which corresponds exactly to the coordinate transformation to apply for modifying the structure of the differential model induced by the u_1 -variable of the Rössler system in such a way that it belongs to the library. The structure selection then works as for the u_3 -variable (Fig. 8(b)) and the coefficients with the indices

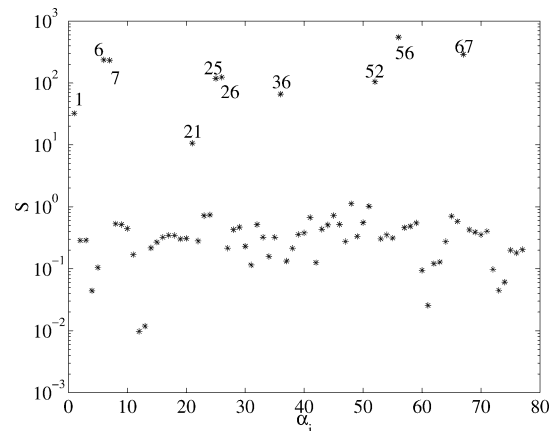
$$\{1, 6, 7, 21, 25, 26, 36, 52, 56, 67\}$$

are selected. They corresponds to monomials

$$\left\{ 1, X, X^2, Y, \frac{Y}{X}, XY, \frac{Y^2}{X}, Z, XZ, \frac{YZ}{X} \right\}. \tag{B.1}$$



(a) Versus Δ



(b) With $\Delta = -4.398$

Fig. 8. Significance of the coefficients α_n computed from the time series $s = u_1 + \Delta$ for different values of Δ (a) and for $\Delta = -4.398$ (b).

All these monomials are involved in the differential models D_l with $l = \{1, 10, 11, 14, 15, 16, 19, 20\}$. Once the structure is selected, the coefficients may be estimated easily (note that one threshold is necessary here since the time series is not spiky). The Rössler system with the rigid displacement ($x \mapsto x - \mathcal{C} + a, y \mapsto y, z \mapsto z$) is

$$\begin{aligned} \dot{x} &= -y - z, \\ \dot{y} &= a - \mathcal{C} + x + ay, \\ \dot{z} &= b + az + xz. \end{aligned} \tag{B.2}$$

The differential model induced by the x -variable then reads as:

$$\begin{aligned}
\dot{X} &= Y, \\
\dot{Y} &= Z, \\
\dot{Z} &= ab + a(a - C) + (2a - C)X + X^2 - a^2Y \\
&\quad + \frac{bY}{X} + \frac{(a - C)Y}{X} - aXY - \frac{aY^2}{X} \\
&\quad + 2aZ + XZ + \frac{YZ}{X}. \tag{B.3}
\end{aligned}$$

This system is a sum of monomials only because $b_2 = c_3 = a$. Such special cases have to be added to the Ansatz Library. The question, how more complex transformations of the observed state variable change the differential model are still under investigation.

References

- [1] F. Takens, in: *Lecture Notes in Mathematics*, Vol. 898, Springer, Berlin, 1981, p. 366.
- [2] N.H. Packard, J.P. Crutchfield, J.D. Farmer, R.S. Shaw, *Phys. Rev. Lett.* 45 (1980) 712.
- [3] T. Sauer, J.A. Yorke, M. Casdagli, *J. Stat. Phys.* 65 (1991) 579.
- [4] J. Crutchfield, B. McNamara, *Complex Systems* 1 (3) (1987) 417.
- [5] D. Broomhead, G. King, *Physica D* 20 (1986) 217.
- [6] J.F. Gibson, J.D. Farmer, M. Casdagli, S. Eubank, *Physica D* 57 (1992) 1.
- [7] C. Lainscsek, C. Letellier, F. Schürerer, *Phys. Rev. E* 64 (2001) 016206.
- [8] G. King, I. Stewart, *Physica D* 58 (1992) 216.
- [9] C. Letellier, G. Gouesbet, *J. Phys. II (Paris)* 6 (1996) 1615.
- [10] D. Kugiumtzis, *Physica D* 95 (1996) 13.
- [11] C. Letellier, J. Maquet, L. Le Sceller, G. Gouesbet, L. Aguirre, *J. Phys. A* 31 (1998) 7913.
- [12] G. Gouesbet, C. Letellier, *Phys. Rev. E* 49 (1994) 4955.
- [13] L. Aguirre, S. Billings, *Int. J. Bifurc. Chaos* 5 (1994) 449.
- [14] K. Judd, A. Mees, *Physica D* 120 (1998) 273.
- [15] L. Le Sceller, C. Letellier, G. Gouesbet, *Phys. Rev. E* 60 (2) (1999) 1600.
- [16] C. Lainscsek, I. Gorodnitsky, F. Schürerer, in preparation (2003).
- [17] L. Aguirre, U. Freitas, C. Letellier, J. Maquet, *Physica D* 158 (2001) 1.
- [18] C. Lainscsek, I. Gorodnitsky, http://cloe.ucsd.edu/claudia/poster_DD_2002.pdf.
- [19] R. Eichhorn, S. Linz, P. Hänggi, *Phys. Rev. E* 58 (6) (1998) 7151.
- [20] W. Press, B. Flannery, S. Teukolsky, W. Vetterling, *Numerical Recipes in C*, Cambridge Univ. Press, 1990.
- [21] B. Bezruchko, T. Dikanev, D. Smirnov, *Phys. Rev. E* 64 (2002) 036210.
- [22] O.E. Rössler, *Phys. Lett. A* 57 (1976) 397.
- [23] C. Letellier, P. Dutertre, B. Maheu, *Chaos* 5 (1) (1995) 271.
- [24] D. Goldberg, *Genetic Algorithms in Search, Optimization and Machine Learning*, Addison–Wesley, Reading, MA, 1998.
- [25] J.H. Holland, *Adaptation in Natural and Artificial Systems*, MIT Press, Cambridge, MA, 1992.